Neuroscience Research 213 (2025) 128–137

Contents lists available at ScienceDirect

Neuroscience Research

journal homepage: www.sciencedirect.com/journal/neuroscience-research

The potential mechanism maintaining transactive response DNA binding protein 43 kDa in the mouse stroke model

Yuting Bian, Yusuke Fukui, Ricardo Satoshi Ota-Elliott, Xinran Hu, Hongming Sun, Zhihong Bian, Yun Zhai, Haibo Yu, Xiao Hu, Hangping An, Hongzhi Liu, Ryuta Morihara, Hiroyuki Ishiura, Toru Yamashita *

Department of Neurology, Graduate School of Medicine, Dentistry and Pharmaceutical Sciences, Okayama University, 2-5-1 Shikata-cho, Kita-Ku, Okayama 700-8558, Japan

ARTICLE INFO

Keywords:
TDP-43
ALS
RNA-binding protein
Mislocalization
G3BP1
HDAC6
RAD23B
tMCAO

ABSTRACT

The disruption of transactive response DNA binding protein 43 kDa (TDP-43) shuttling leads to the depletion of nuclear localization and the cytoplasmic accumulation of TDP-43. We aimed to evaluate the mechanism underlying the behavior of TDP-43 in ischemic stroke. Adult male C57BL/6 J mice were subjected to 30 or 60 min of transient middle cerebral artery occlusion (tMCAO), and examined at 1, 6, and 24 h post reperfusion. Immunostaining was used to evaluate the expression of TDP-43, G3BP1, HDAC6, and RAD23B. The total and cytoplasmic number of TDP-43–positive cells increased compared with sham operation group and peaked at 6 h post reperfusion after tMCAO. The elevated expression of G3BP1 protein peaked at 6 h after reperfusion and decreased at 24 h after reperfusion in ischemic mice brains. We also observed an increase of expression level of HDAC6 and the number of RAD23B-positive cells increased after tMCAO. RAD23B was colocalized with TDP-43 24 h after tMCAO. We proposed that the formation of stress granules might be involved in the mislocalization of TDP-43, based on an evaluation of G3BP1 and HDAC6. Subsequently, RAD23B, may also contribute to the downstream degradation of mislocalized TDP-43 in mice tMCAO model.

1. Introduction

Transactive response DNA binding protein 43 kDa (TDP-43) is widely known as an RNA-binding protein that is closely associated with multiple chronic neurodegenerative diseases, including amyotrophic lateral sclerosis (ALS) and frontotemporal lobar degeneration (FTLD) (Arai et al., 2006; Barmada et al., 2010; Chhangani et al., 2021; Neumann et al., 2006; Prasad et al., 2019; Scotter et al., 2015; Suk et al., 2020). It performs several mRNA-related processes in the nucleus, such as transcription, splicing, and maintaining RNA stability (Prasad et al., 2019). TDP-43 is predominantly located in the nucleus in normal conditions, and can shuttle between the nucleus and cytoplasm (Watanabe et al., 2020). However, disruption of this shuttling under pathological conditions leads to the loss of functional TDP-43 in the nucleus and increased deposition in cytoplasmic inclusions in the brain and spinal cord neurons, which are characteristic pathological findings in ALS and FTLD-TDP (Ederle et al., 2017; Prasad et al., 2019). TDP-43 mislocalization may be the initial step in the neurodegenerative process of ALS (Suk et al., 2020). Consequently, there has been considerable focus on whether pathological changes in TDP-43 can be observed in other

Abbreviations: ALS, amyotrophic lateral sclerosis; BSA, bovine serum albumin; CHIP, carboxyl terminus of Hsp70-interacting protein; DAB, diaminobenzidine tetrahydrochloride; ER, endoplasmic reticulum; FTLD, frontotemporal lobar degeneration; G3BP1, GTPase activating protein binding protein 1; HDAC6, histone deacetylase 6; Hsc70, heat-shock cognate 70; Hsp70, heat-shock protein 70; IntDen, integrated density; I/R, ischemia/reperfusion; MCA, middle cerebral artery; MRP, microtubule-related protein; PBS, phosphate-buffered saline; PFA, paraformaldehyde; RBP, RNA-binding protein; ROI, region of interest; RT, room temperature; S.D., standard deviation; SG, stress granule; TDP-43, transactive response DNA binding protein 43 kDa; tMCAO, transient middle cerebral artery occlusion; TNB, Tris-NaCl-blocking; Ub, ubiquitin; UPS, ubiquitin-proteasome system.

* Corresponding author.

E-mail addresses: pynw8tow@s.okayama-u.ac.jp (Y. Bian), yfukui@s.okayama-u.ac.jp (Y. Fukui), pyhm8xf3@s.okayama-u.ac.jp (R.S. Ota-Elliott), pud386d6@s.okayama-u.ac.jp (X. Hu), pt6r8bnx@s.okayama-u.ac.jp (H. Sun), puyd4cmh@s.okayama-u.ac.jp (Z. Bian), zntsjzy@outlook.com (Y. Zhai), p96b4sd9@s.okayama-u.ac.jp (H. Yu), phbm1rpq@s.okayama-u.ac.jp (X. Hu), plsu5s0z@s.okayama-u.ac.jp (H. An), p18q8iu8@s.okayama-u.ac.jp (H. Liu), rmorihara@okayama-u.ac.jp (R. Morihara), ishiura@s.okayama-u.ac.jp (H. Ishiura), toruyamashita@okayama-u.ac.jp (T. Yamashita).

https://doi.org/10.1016/j.neures.2025.01.006
Received 8 October 2024; Received in revised form 21 January 2025; Accepted 26 January 2025
Available online 29 January 2025

neuropathological conditions. Elevated TDP-43 has been reported after ischemic stroke in the transient middle cerebral artery occlusion (tMCAO) rodent model (Kahl et al., 2018; Kanazawa et al., 2011; Liu et al., 2020). However, the existing mechanisms underlying this phenomenon are not fully understood.

Under stress conditions, such as ischemia/reperfusion injury, protein synthesis, folding, and degradation are interrupted, leading to the deposition of aggregated proteins and ultimately, cell death (Chhangani et al., 2021; Kahl et al., 2018; Lei et al., 2021). During stalled protein translation under stress conditions, stress granules (SGs) may form, and GTPase activating protein binding protein 1 (G3BP1) triggers phase separation to assemble SGs (Yang et al., 2020), which protect cells under acute stress stimuli (Wolozin et al., 2019), while histone deacetylase 6 (HDAC6) promotes the formation of SGs and transports proteins that have lost degradation homeostasis (Kawaguchi et al., 2003; Kwon et al., 2007), with the aim of restoring homeostasis. Molecular chaperones, such as co-chaperone carboxyl terminus of Hsp70-interacting protein (CHIP), heat-shock cognate 70 (Hsc70), and heat-shock protein 70 (Hsp70), can recognize ubiquitinated, mislocalized, or misfolded proteins, based on different characteristics such as misfolding, size, and solubility (Ciechanover et al., 2015; Lei et al., 2021). These chaperones direct the substrates to the protein degradation system, which includes the ubiquitin (Ub)-proteasome system (UPS). RAD23 homolog B (RAD23B) can act as a substrate shuttling factor, triggering a liquid-liquid phase separation (LLPS) (Ciechanover et al., 2015; Lei et al., 2021; Yasuda et al., 2020).

The aim of this study was to investigate the potential mechanism of mislocalized TDP-43 under stress conditions by evaluating changes in the expression levels of G3BP1, HDAC6, and RAD23B in the tMCAO mice model.

2. Materials and methods

2.1. Animals and experimental groups

Adult male C57BL/ 6 J mice (23–29 g, 8–11 weeks old) were used in this study (Japan SLC Inc., Shizuoka, Japan). The mice were acclimatized to standard mice cages under conventional laboratory conditions with a 12/12 hours (h) light/dark cycle and constant humidity with regular room temperature (RT) (23–25°C), and allowed free access to food and water. Mice were randomly assigned to three experimental groups, including the sham operation group, the 30 minute (min) transient middle cerebral artery occlusion (tMCAO) group, and the 60 min tMCAO group, each of which contained three sacrifice time points at 1, 6, and 24 h post sham operation/reperfusion.

All experimental procedures were certified by the Animal Committee of the Okayama University Graduate School of Medicine (OKU-2021406) and conducted according to ARRIVE guidelines (https://www.nc3rs.org.uk/arriveguidelines) and the Okayama University guidelines for the Care and Use of Laboratory Animals.

2.2. Focal cerebral ischemia

Transient focal ischemia was induced by right middle cerebral artery (MCA) occlusion. During surgery, mice were anesthetized by inhalation of a mixture of nitrous oxide, oxygen, and isoflurane (69/30/1 %), using a face mask. tMCAO was induced by the intraluminal filament technique (Abe et al., 1992; Yamashita et al., 2006). Briefly, the right carotid bifurcation was exposed, a silicone-coated 7–0 filament was inserted into the right internal cerebral artery and gently advanced (8.0–9.0 mm) to occlude the MCA. After 30 or 60 min of occlusion, the filament was gently withdrawn to restore blood flow. For sham-operated mice, all steps of cervical surgery were conducted except for insertion of the nylon thread. The body temperature of mice during surgery was maintained at 36.5°C ± 0.5°C using a heating pad (model BMT-100; Bio Research Center, Tokyo, Japan) (Shang et al., 2018).

2.3. Tissue preparation

The number of mice in each experimental group is shown in Fig. 1a. Each mouse was anesthetized by intraperitoneal injection of pentobarbital (20 mg/kg) and then perfused with chilled phosphate-buffered saline (PBS), followed by 4 % paraformaldehyde (PFA) in 0.1 mol/L phosphate buffer. After post-fixation overnight, the mice brain samples were subsequently washed with PBS, then the tissues were sequentially transferred into 10, 20, and 30 % (wt/vol) sucrose solutions. Tissues were embedded in O.C.T.™ compound (Tissue-Tek® O.C.T.™ Compound) and stored at −80℃. Tissues were then cut into 20 μm-thick sections with a cryostat (HM525 NX, Thermo Fisher Scientific, USA) (Nakano et al., 2017).

2.4. Immunohistochemistry and infarct volume

Frozen sections were incubated in 4 % PFA for 15 min at RT. After washing in PBS, the sections were pretreated with 10 mM citrate acid buffer (pH 6.0) for antigen retrieval. After washing in PBS, sections were then incubated in 1 % hydrogen peroxide/methanol for 20 min. After washing in PBS again, brain sections were blocked in a mixture of 5 % bovine serum albumin (BSA, Sigma-Aldrich, A3059) and 0.1 % (final concentration) Triton™ X-100 for 1 h at RT, then incubated at 4℃ overnight with a mixture of primary antibodies: rabbit anti-MAP2 antibody (1:500, Abcam, ab32454), rabbit anti-HDAC6 antibody (1:100, Abcam, ab1440), and rabbit anti-RAD23B antibody (1:300, Proteintech, 12121–1-AP). Sections were then washed in PBS and incubated with biotin-labeled secondary antibody (1:500, within the VECTASTAIN® ABC-HRP Kit, PK 4001; Vector Laboratories, Inc., Newark, CA, USA) for 2 h, then incubated with prepared VECTASTAIN ABC Reagent (within the VECTASTAIN® ABC-HRP Kit, PK-4001). For the mouse anti-TDP-43 antibody (1:200; Santa Cruz, Dallas, TX, USA; sc-376532), the Mouse on Mouse (M.O.M.) basic kit (Vector Laboratories, BMK-2202) was used for masking endogenous mouse antigen. The signal was then visualized with diaminobenzidine tetrahydrochloride (DAB tablets; Wako Chemicals, Richmond, VA, USA; 045–22833). Sections were observed under a light microscope (SZX-12; Olympus Optical, Tokyo, Japan). For quantitative analysis of cerebral infarct volume, five serial brain slices from each mouse were selected at a 0.5 mm interval, between + 0.98 mm anterior and −0.94 mm posterior to the bregma. We detected the ischemic area based on the loss of MAP2-positive neuropils, and the ischemic core was defined as the absence of MAP2 immunoreactivity while perilesional sites were defined as areas that attenuated the MAP2 signal (Popp et al., 2009; Tachibana et al., 2017; Shibahara et al., 2020). Infarct area was measured using Image J software (National Institutes of Health, Bethesda, MD, USA). Infarct volume of each brain was calculated by adding infarct areas of the five serial brain slices (Nakano et al., 2017). To evaluate sections immunostained for TDP-43, HDAC6, and RAD23B, three areas of the peri-infarct cortex from each of three coronal levels between + 0.98 mm anterior and + 0.02 mm posterior to the bregma, were chosen randomly and captured at × 200 magnification with a light microscope (BX51; Olympus, Tokyo, Japan). ImageJ was used to assess the average number of positively expressed cells of either the nuclei or cytoplasmic patterns of TDP-43 or HDAC6, the number of RAD23B–positive cells, as well as pixel intensity, which was evaluated within the region of interest (ROI). ROI was selected by a threshold in each capture (0.12 mm^2).

2.5. Immunofluorescence analysis

For immunofluorescent staining, sections were blocked in 0.5 % Tris-NaCl-blocking (TNB) buffer (Perkin Elmer, FP1012) for 1 h at RT. These were then incubated at 4℃ overnight with the following primary antibodies: mouse anti-TDP-43 antibody (1:100, Santa Cruz, sc-376532), rabbit anti-G3BP1 antibody (1:500, Proteintech, 13057–2-AP), and rabbit anti-RAD23B antibody (1:300, Proteintech, 12121–1-AP). The

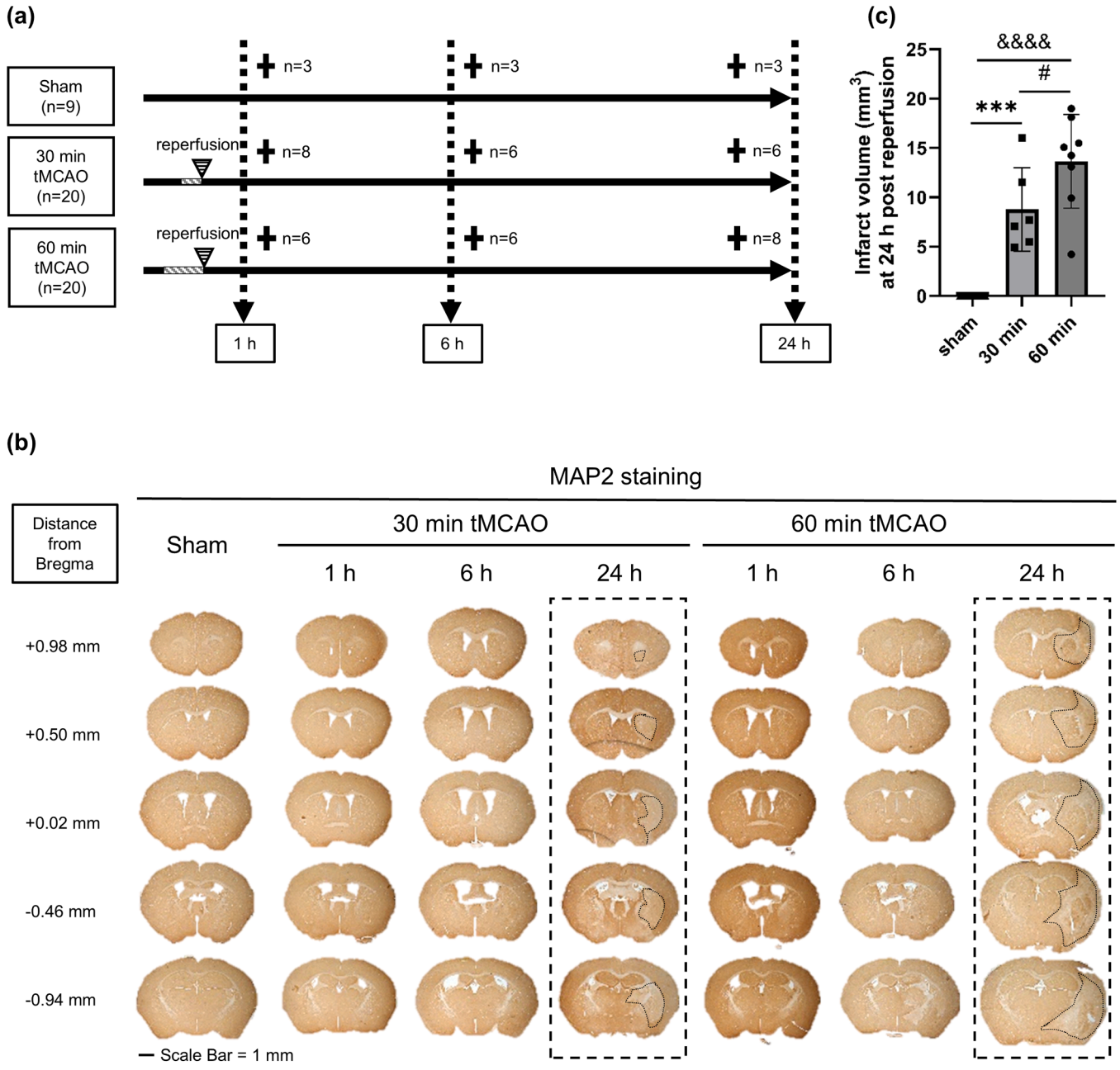

Fig. 1. Experimental time course and cerebral ischemia after tMCAO surgery. (a) Mice were divided into three groups, sham operation, 30 min, and 60 min tMCAO, and sacrificed at 1, 6, and 24 h after reperfusion. (b) Representative anti-MAP2 staining sections, showing the ischemic area at different reperfusion time points after tMCAO. (c) There were significant increases in infarct volume depending on occlusion time at 24 h after tMCAO (***, $P < 0.001$ 30 min group versus sham group; &&&&, $P < 0.0001$ 60 min group versus sham group; #, $P < 0.05$ 60 min group versus 30 min group; one-way ANOVA with the Tukey-Kramer multiple comparisons test). Scale bar = 1 mm.

sections were washed in PBS and incubated with appropriate secondary antibodies. Three levels of sections were selected from three coronal levels: + 0.98 mm, + 0.50 mm, and + 0.02 mm rostral to the bregma. Three areas in the ipsilateral peri-infarcted lesion in each section were chosen randomly and images were captured with a confocal laser microscope (LSM780; Carl Zeiss AG, Oberkochen, Germany). The average integrated density (IntDen) of TDP-43 or G3BP1 was evaluated as TDP-43/G3BP1 double immunofluorescence by ImageJ.

2.6. Quantitative and statistical analyses

Data was analyzed using GraphPad Prism version 10.0.0 for Windows (GraphPad Software, Boston, MA, USA). Data is displayed as the mean ± standard deviation (S.D.). We performed a one-way analysis of variance (ANOVA) followed by the Tukey-Kramer multiple comparisons test to compare infarct volume. We also performed a two-way ANOVA followed by the Tukey-Kramer multiple comparisons test to compare immunopositive cell numbers, IntDen, and pixel intensity among the nine independent experimental groups categorized by reperfusion and sacrificing time. To assess the correlation of IntDen between TDP-43 and G3BP1, Spearman's correlation coefficient test was performed. *P*-values < 0.05 were considered to be significantly different.

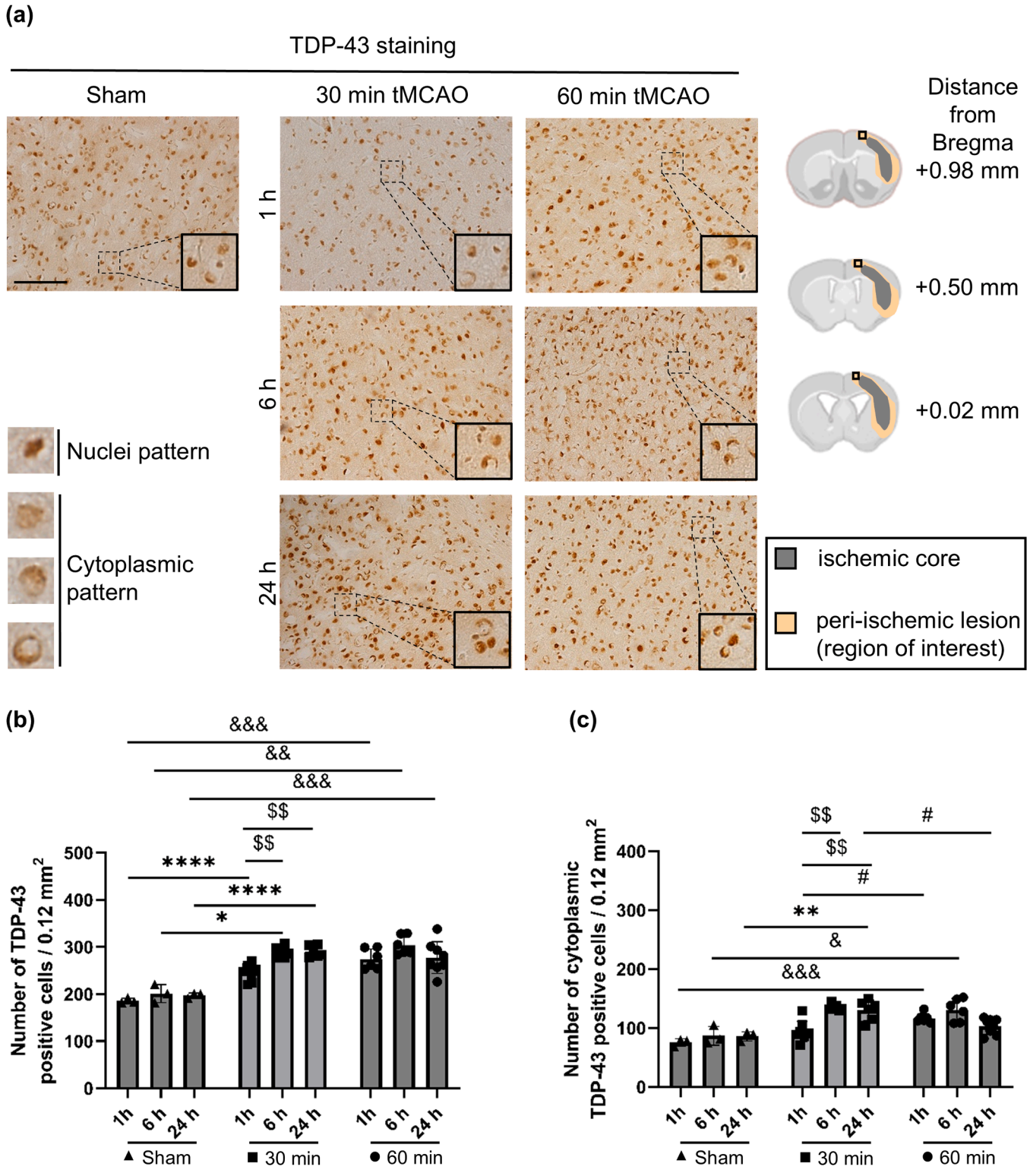

Fig. 2. Total and cytoplasmic TDP-43–positive cells increased after tMCAO. (a) Immunohistochemistry for TDP-43 at the peri-ischemic lesion and schema of the chosen sections. Schematic diagram of mice brain coronal section was created with BioRender.com. (b) Quantitative analyses of total number of TDP-43–positive cells. (c). Quantitative analyses of cytoplasmic TDP-43–positive cell number. Scale bar = 200 μm (*, **, and ****, $P < 0.05$, $P < 0.01$, and $P < 0.0001$, respectively, in 30 min tMCAO group versus sham group; &, && and &&&, $P < 0.05$, $P < 0.01$ and $P < 0.001$, respectively, in 60 min tMCAO group versus sham group; #, $P < 0.05$ in 60 min versus 30 min tMCAO group; $$, $P < 0.01$ in 30 min tMCAO group; two-way ANOVA with the Tukey-Kramer multiple comparisons test).

3. Results

3.1. Experimental time course and cerebral ischemia after tMCAO surgery

MAP2 proved to be an excellent marker at all post-ischemic times examined, and its early sensitivity is an obvious advantage, as has been confirmed by several studies (Popp et al., 2009; Shibahara et al., 2020; Tachibana et al., 2017). Among the three groups in Fig. 1a, no clear infarct lesions could be identified during anti-MAP2 staining at 1 h and 6 h after tMCAO (Fig. 1b). Conversely, there were significant increases in infarct volume, depending on occlusion time, at 24 h after tMCAO (sham: 0 mm^3; 30 min: 8.8 ± 4.2 mm^3; 60 min: 13.6 ± 4.7 mm^3;

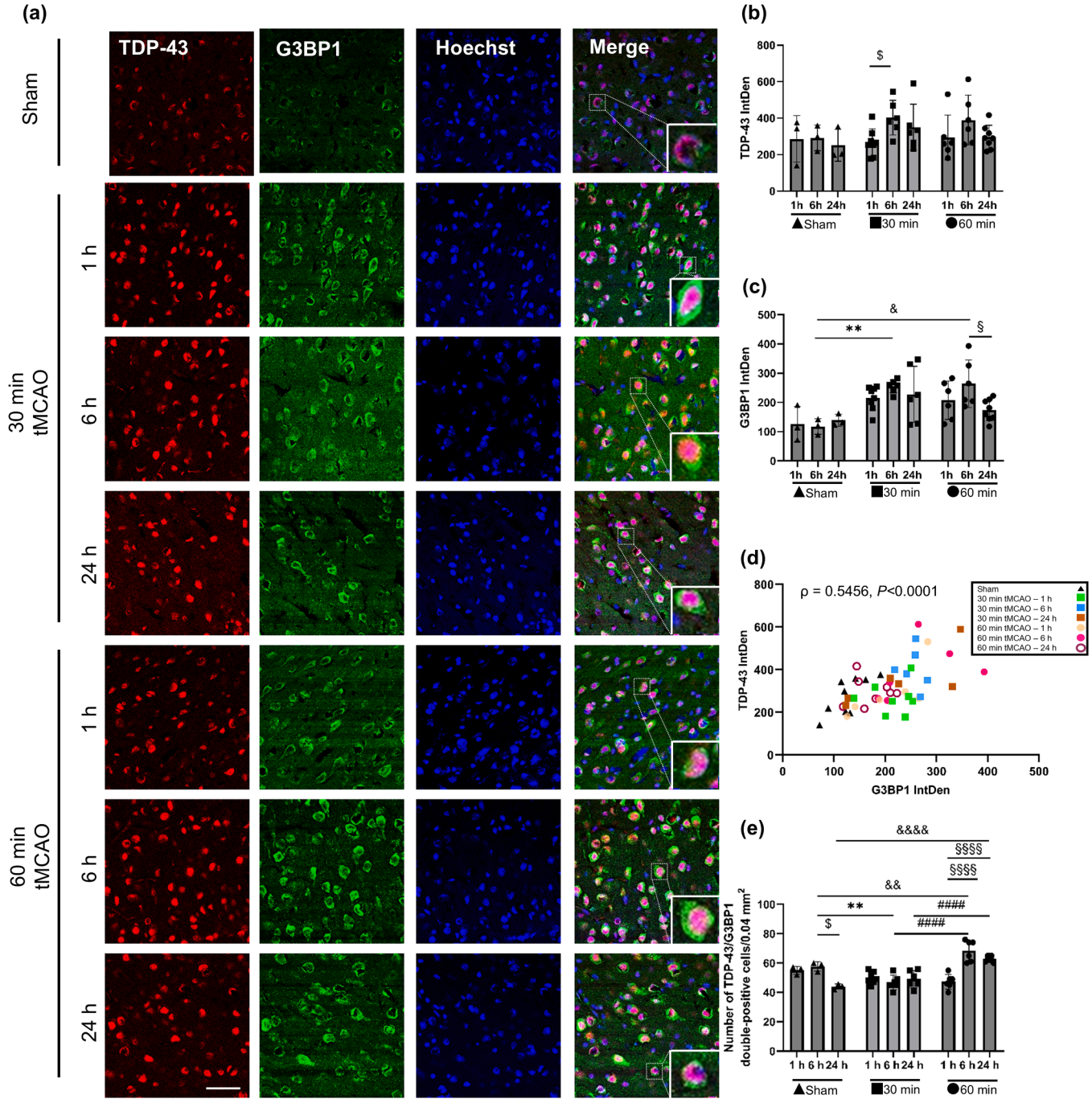

Fig. 3. TDP-43 expression changed in parallel with G3BP1 expression. (a) Double immunofluorescence analysis for TDP-43 and G3BP1. Representative results are shown. (b) Quantitative analysis of TDP-43 immunofluorescence analysis by integrated density (IntDen). TDP-43 expression increased significantly in the cortical penumbra area and peaked at 6 h post reperfusion in both 30 min and 60 min tMCAO groups, followed by a decreasing trend in both tMCAO groups. (c) Quantitative analysis of G3BP1 immunofluorescence analysis by IntDen. (d) A scatter diagram of the TDP-43 IntDen and G3BP1 IntDen. G3BP1 expression increased as did TDP-43 expression (ρ= 0.5456, $P < 0.0001$; Spearman's correlation coefficient test). (e) Quantitative analysis of TDP-43/G3BP1 double-positive cells. Significant differences were observed between 6 h and 24 h after 60 min tMCAO groups compared with the sham operation group in each visual field. Significant differences were also observed between 6 h and 24 h after 60 min tMCAO groups compared with 30 min tMCAO groups (**, $P < 0.01$ in 30 min tMCAO group versus sham group; &, &&, &&&&, $P < 0.05$, $P < 0.01$, and $P < 0.0001$ in 60 min tMCAO group versus sham group; $, $P < 0.05$ in 30 min tMCAO group; §, §§§§, $P < 0.05$ and $P < 0.0001$ in 60 min tMCAO group; two-way ANOVA with the Tukey-Kramer multiple comparisons test).

Fig. 1c).

3.2. Increase in the number of total and cytoplasmic TDP-43–positive cells after tMCAO

The TDP-43 protein is predominantly localized in the nucleus and can shuttle between the nucleus and cytoplasm (Barmada et al., 2010; Lee et al., 2020). Studies have shown that the cytoplasmic accumulation of TDP-43 aggregates is one of the major characteristics of TDP-43 proteinopathy, including ALS and FTLD-TDP (Kim et al., 2014; Scotter et al., 2015; Shenouda et al., 2018). First, we investigated the total and cytoplasmic number of TDP-43–positive cells during post cerebral ischemia/reperfusion (I/R) injury in mice brain tissue (Fig. 1a). The average total number of TDP-43–positive cells per visual field in 30 min or 60 min tMCAO groups increased significantly compared to cells in the same sacrificial time points of the sham operation group (sham group: 1 h, 186.0 ± 5.3; 6 h, 201.0 ± 19.0; 24 h, 197.3 ± 5.5; 30 min tMCAO group: 1 h, 246.3 ± 17.4; 6 h, 289.0 ± 11.8; 24 h: 290.8 ± 11.9; 60 min tMCAO group: 1 h, 274.5 ± 21.7; 6 h, 303.8 ± 20.4; 24 h: 277.8 ± 33.8. $P < 0.05$ in 30 min tMCAO group versus sham group; $P < 0.05$ in 60 min tMCAO group versus sham group; Fig. 2b). Interestingly, there were significant differences in 6 h and 24 h after 30 min tMCAO groups compared with the 1 h group. A similar trend was observed in the number of cytoplasmic TDP-43–positive cells per visual field (sham group: 1 h, 75.3 ± 6.4; 6 h, 87.0 ± 15.9; 24 h, 86.0 ± 7.9; 30 min tMCAO group: 1 h, 94.4 ± 17.0; 6 h, 135.2 ± 5.5; 24 h: 130.2 ± 17.4; 60 min tMCAO group: 1 h, 116.8 ± 8.1; 6 h, 130.7 ± 19.2; 24 h: 102.9 ± 13.6; Fig. 2c).

3.3. TDP-43 expression changed in parallel with G3BP1 expression

GTPase activating protein binding protein 1 (G3BP1) localizes to SGs (Si et al., 2020; Wolozin et al., 2019). To study the re-localization of endogenous or ectopically expressed TDP-43 to SGs in response to I/R attack post-tMCAO in mice brains, we conducted double immunofluorescence staining of TDP-43 and G3BP1. The IntDen of either TDP-43 or G3BP1 was significantly higher in the cortical penumbra area and peaked at 6 h post reperfusion, in both 30 min and 60 min tMCAO groups, also followed by a decreasing trend in both tMCAO groups (Fig. 3a–c).

We also analyzed the overall correlation between IntDens of TDP-43 and G3BP1 in all groups (Spearman's ρ=0.5456, $^*P < 0.0001$. Fig. 3d). The Spearman's correlation results of the 60 min occlusion group between IntDens of TDP-43 and G3BP1 showed a stronger relationship using a monotonic function than that of the 30 min occlusion group (Spearman's ρ=0.5233, $P = 0.0179$ in the 30 min tMCAO group and Spearman's ρ=0.6391, $P = 0.0024$ in the 60 min tMCAO group). We then analyzed the double-positive cell number of TDP-43 and G3BP1. Significant differences were observed between 6 h and 24 h after 60 min tMCAO groups compared with the sham operation group in each visual field. Significant differences were also observed between 6 h and 24 h after 60 min tMCAO groups compared with the 30 min tMCAO groups, indicating that double-positive cell numbers of TDP-43/G3BP1 might be related with the severity of tMCAO (sham group: 1 h, 55.0 ± 2.6; 6 h, 57.7 ± 3.2; 24 h, 43.9 ± 1.8; 30 min tMCAO group: 1 h, 50.0 ± 4.0; 6 h, 46.8 ± 5.0; 24 h: 49.2 ± 5.8; 60 min tMCAO group: 1 h, 47.3 ± 5.0; 6 h, 68.3 ± 7.2; 24 h: 62.9 ± 2.0; Fig. 3e).

3.4. HDAC6 total positive cell number and its cytoplasmic pattern were both upregulated after tMCAO

HDAC6 has been shown to be involved in the sequestration of TDP-43 into microtubule-related protein (MRP)-induced aggregates in the cytoplasm (Watanabe et al., 2020). Single immunohistochemical staining of HDAC6 revealed that the average number of total HDAC6-positive cells per visual field increased after tMCAO in the 30 min tMCAO group (1 h, 97.4 ± 22.6; 6 h, 111.5 ± 21.0; 24 h, 116.2 ± 23.0), but increased significantly in the 60 min tMCAO group (1 h: 118.0 ± 9.7, 6 h: 93.0 ± 18.5, 24 h: 137.1 ± 17.1) compared with the sham operation group (1 h: 45.5 ± 4.6, 6 h: 46.0 ± 3.4, 24 h: 50.0 ± 5.3, $P < 0.05$ in 30 min tMCAO group versus sham group; $P < 0.05$ in 60 min tMCAO group versus sham group; Fig. 4b). The increase in the average number of cytoplasmic HDAC6-positive cells per visual field was also observed in the 30 min tMCAO group (1 h: 62.9 ± 18.2, 6 h: 70.5 ± 19.4, 24 h: 73.7 ± 13.4), and in the 60 min tMCAO group (1 h:77.7 ± 7.9, 6 h: 61.8 ± 12.8, 24 h: 92.6 ± 13.3), when compared with the sham operation group (1 h: 28.5 ± 3.2, 6 h: 30.9 ± 2.9, 24 h: 35.0 ± 5.6, $P < 0.05$ in 30 min tMCAO group versus sham group; $P < 0.05$ in 60 min tMCAO group versus sham group; Fig. 4c).

3.5. Total positive cell number and pixel intensity of proteasomal degradation marker RAD23B were upregulated after tMCAO

Changes in the expression of RAD23B, a novel substrate-shuttling factor for the proteasome, might indicate the degradation of mislocalized/misfolded protein (Yasuda et al., 2020). RAD23B plays a central role in both proteasomal degradation of misfolded proteins and DNA repair (Schärer et al., 2013; Yasuda et al., 2020), so it might display a shift between the nucleus and cytoplasm. To explore whether this protein takes part in TDP-43 degradation in mice brain tissue, anti-RAD23B immunohistochemistry staining was conducted (Fig. 5a). Average RAD23B-positive cell number per visual field increased in the 30 min tMCAO group (1 h: 99.9 ± 24.8, 6 h: 101.0 ± 15.6, 24 h: 125.3 ± 20.8. $P < 0.05$ in 30 min tMCAO group versus sham group) and in the 60 min tMCAO group (1 h: 148.0 ± 15.6, 6 h: 130.7 ± 19.5, 24 h: 157.0 ± 14.5. $P < 0.05$ in 60 min tMCAO group versus sham group; Fig. 5b), compared with the sham operation group (1 h: 51.7 ± 8.1, 6 h: 60.3 ± 7.0, 24 h: 69.7 ± 11.6). The total number of RAD23B-positive cells per visual field increased significantly with ischemic severity ($P < 0.05$ in the 30 min tMCAO group versus the 60 min tMCAO group; Fig. 5b). The pixel intensity of RAD23B also indicated that upregulation had occurred in both the 30 min and 60 min tMCAO groups (Fig. 5c).

To examine the colocalization of TDP-43 and RAD23B, double immunofluorescence staining was performed at 24 h after tMCAO. The analysis revealed that TDP-43–positive cells strongly co-expressed the proteasomal degradation marker, RAD23B, at 24 h after both 30 min tMCAO and 60 min tMCAO (Fig. 5d). We also performed TDP-43 and RAD23B double-positive cell quantification using a visual field analysis. There were significant differences between 24 h after 30 min tMCAO compared with the sham operation group, and between 1 h, 6 h, 24 h after 60 min tMCAO compared with the sham operation group (sham group: 1 h, 39.3 ± 11.8; 6 h, 34.3 ± 4.2; 24 h, 30.0 ± 2.6; 30 min tMCAO group: 1 h, 46.9 ± 7.4; 6 h, 43.0 ± 6.4; 24 h: 49.5 ± 6.9; 60 min tMCAO group: 1 h, 51.0 ± 7.0; 6 h, 47.8 ± 5.3; 24 h: 56.8 ± 1.8; Fig. 5e).

4. Discussion

In the present study, we showed that the total and cytoplasmic number of TDP-43–positive cells increased after tMCAO (Fig. 2a–c). Furthermore, the ratio of cytoplasmic TDP-43–positive cells increased in the 60 min tMCAO group at 6 h post reperfusion compared with 1 h, then decreased at 24 h post-reperfusion (60 min tMCAO group: 1 h, 42 %; 6 h, 50 %; 24 h, 43 %). This indicates that the phenomenon of TDP-43 mislocalization also occurs in ischemic mice brains. The expression of either TDP-43 or G3BP1 protein peaked at 6 h after reperfusion then decreased at 24 h after reperfusion (Fig. 3a–e). Moreover, Spearman's correlation within the 60 min occlusion group between IntDens of TDP-43 and G3BP1 showed a better relationship using a monotonic function than that within the 30 min occlusion group. Moreover, an increase in HDAC6 was observed (Fig. 4a–c). HDAC6 promoted TDP-43 aggregation, an increase in the number of RAD23B-

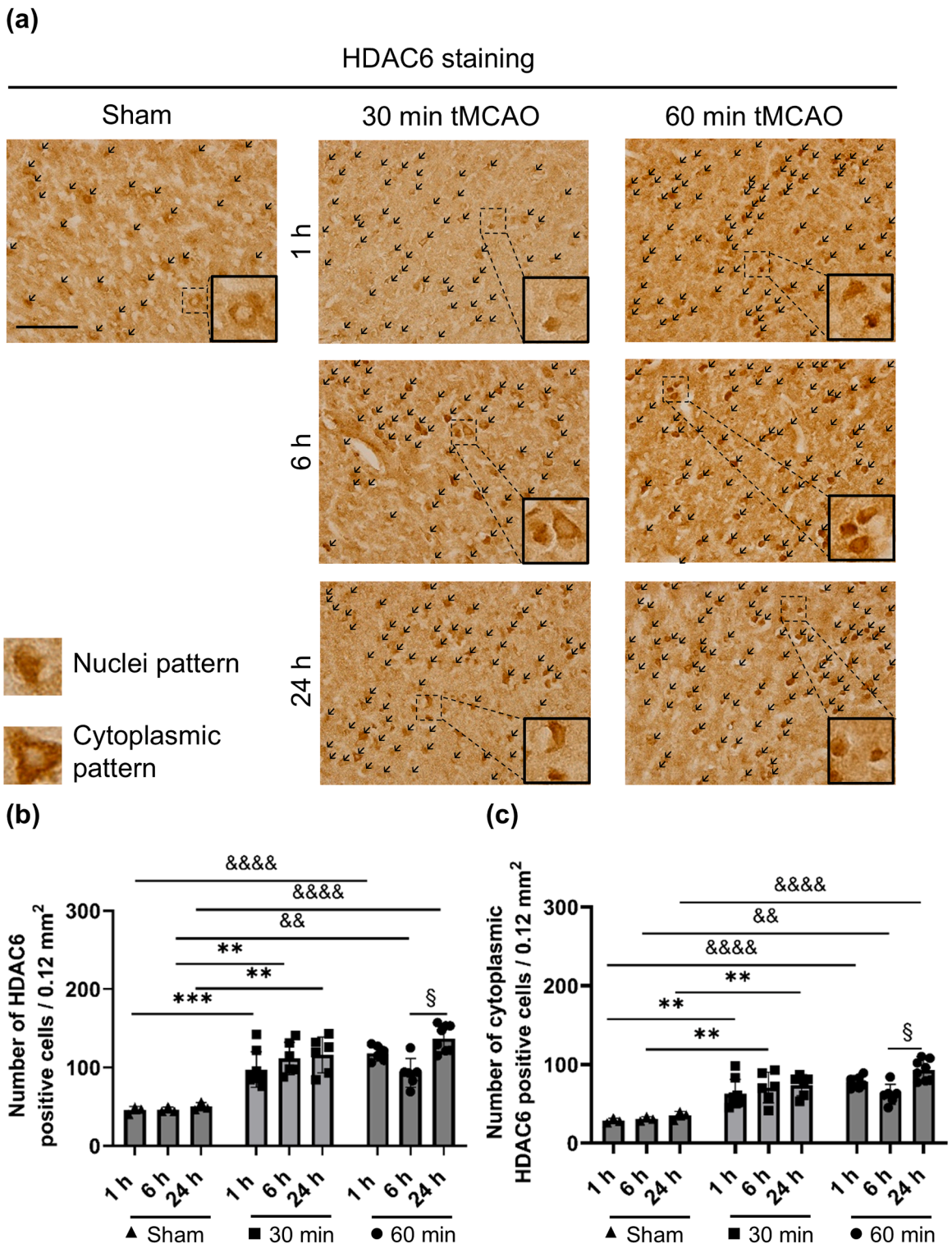

Fig. 4. HDAC6 total positive cell number and its cytoplasmic pattern were both upregulated after tMCAO. (a) Immunohistochemistry for HDAC6 at the peri-ischemic lesion. Black arrows indicate a positive signal. (b) Quantitative analyses of total number of HDAC6-positive cells. (c) Quantitative analyses of number of cytoplasmic HDAC6-positive cells. Scale bar = 200 μm. ** and *** , $P < 0.01$ and $P < 0.001$, respectively, in 30 min tMCAO group versus sham group; && and &&&&, $P < 0.01$ and $P < 0.0001$, respectively, in 60 min tMCAO group versus sham group; §, $P < 0.05$ in 60 min tMCAO group; two-way ANOVA with the Tukey-Kramer multiple comparisons test.

positive cells, a marker of proteasomal degradation, and its co-localization with TDP-43 (Fig. 5a–e).

Previous studies have shown that ischemia/reperfusion induce endoplasmic reticulum (ER) stress, oxidative stress, nuclear transport dysfunction, axonal transport defects, and apoptosis, evoking the pathological aggregation of RNA-binding proteins such as TDP-43 (Chhangani et al., 2021; Kahl et al., 2018). The mislocalization of TDP-43 may be an initial step in the pathological process leading to the formation of TDP-43–positive aggregates observed in neurodegenerative diseases (Keating et al., 2022; Suk and Rousseaux, 2020). Our

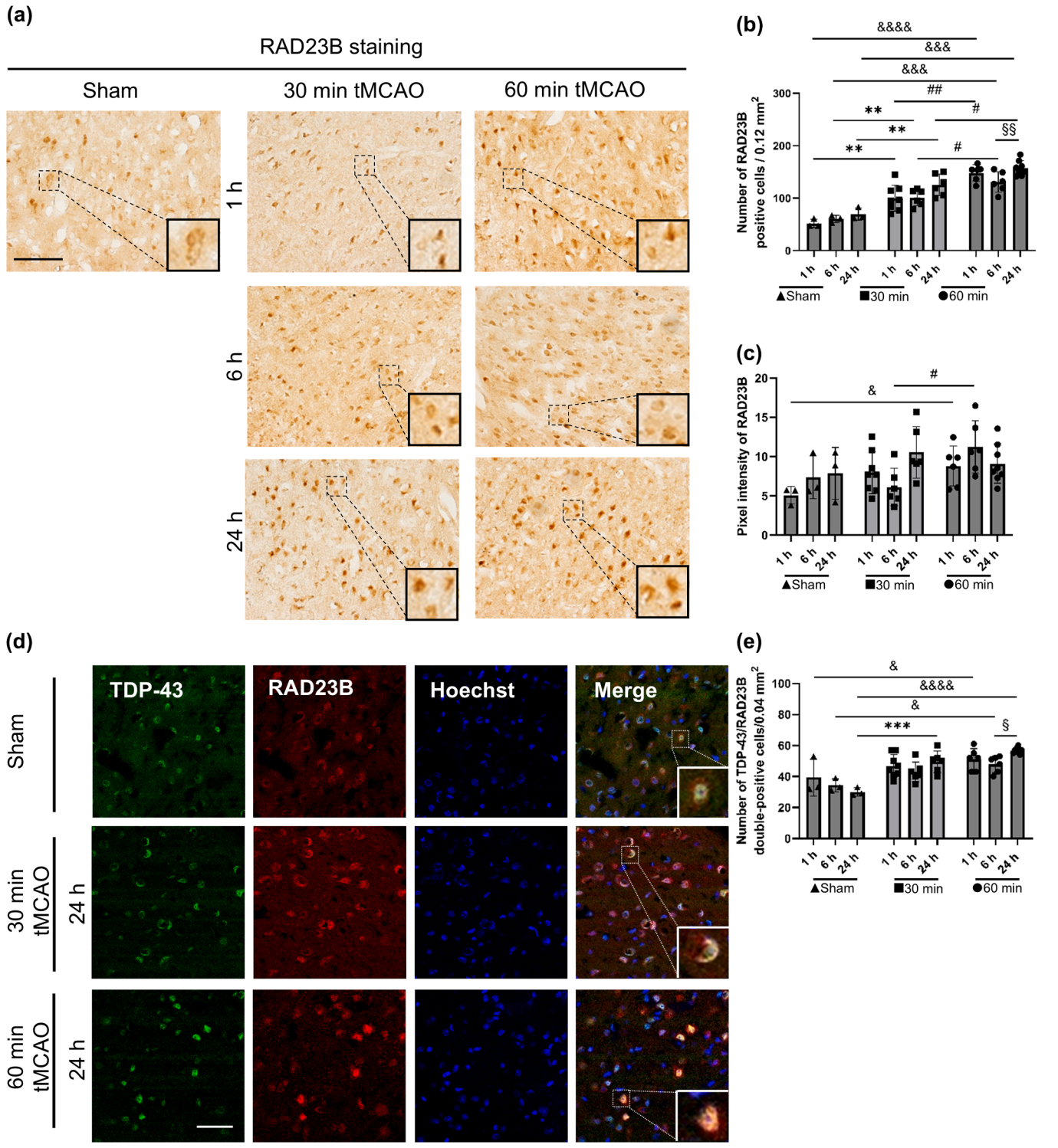

Fig. 5. Total number of positive cells and pixel intensity of proteasomal degradation marker RAD23B were upregulated after tMCAO. (a) Immunohistochemistry for RAD23B at the peri-ischemic lesion. (b) Quantitative analyses of total number of RAD23B-positive cells. (c) Quantitative analyses of RAD23B pixel intensity. Scale bar = 200 μm. (d) Representative double immunofluorescence captures for TDP-43 and RAD23B showed colocalization of TDP-43 and RAD23B at 24 h post reperfusion, either in the 30 min or 60 min tMCAO group. The small panels display a representative double-positive cell. Scale bar = 50 μm. (e) Quantitative analysis of TDP-43/RAD23B double-positive cells per visual field. There were significant differences between 24 h after 30 min tMCAO compared with the sham operation group, and between 1 h, 6 h, 24 h after 60 min tMCAO compared with the sham operation group (** and ***, $P < 0.01$ and $P < 0.001$ in 30 min tMCAO group versus sham group; &, &&&, and &&&&, $P < 0.05$, $P < 0.001$, and $P < 0.0001$, respectively, in 60 min tMCAO group versus sham group; # and ##, $P < 0.05$ and $P < 0.01$ in 60 min versus 30 min tMCAO group; § and §§, $P < 0.05$ and $P < 0.01$ in 60 min tMCAO group; two-way ANOVA with the Tukey-Kramer multiple comparisons test).

results revealed that this type of mislocalization of TDP-43 can occur in the acute ischemic mice brain (Fig. 1, Fig. 2a–c). SGs form rapidly in cells in response to specific stress stimuli, such as hypoxia, malnutrition, and protein denaturation (Aramburu-Núñez et al., 2022; Wolozin et al., 2019). SGs are composed of a complex of mRNA and various protein molecules that are assembled through liquid-liquid phase separation (LLPS) (Boeynaems et al., 2018; Suk and Rousseaux, 2020; Wolozin et al., 2019). SG formation promoted cell survival under stress conditions by suppressing translation but also by sequestering some apoptosis regulatory factors (Arimoto-Matsuzaki et al., 2016). G3BP1 could be one of the core nucleating RNA-binding proteins (RBPs) for SGs, interacting with SGs by directly binding to mRNAs, and facilitating the assembly of SGs (Guillén-Boixet et al., 2020; Sanders et al., 2020; Sidibé et al., 2021; Yang et al., 2020). Endogenous TDP-43 localizes to SGs and regulates their formation and maintenance by controlling the levels of G3BP1 (McDonald et al., 2011). In this study, G3BP1, along with TDP-43, peaked at 6 h after the onset of stroke and then decreased at 24 h. These results indicate that G3BP1 may take part in SG formation with TDP-43 in the acute stroke mice brain (Watanabe et al., 2020). HDAC6 was also reported to be a component of SGs and promotes their formation. HDAC6 removes proteins such as TDP-43 that lose their homeostasis probably by binding to microtubes, promotes aggresome formation, and protects cells from apoptosis following stress (Kawaguchi et al., 2003; Kwon et al., 2007). TDP-43 cooperatively regulated HDAC6 mRNA by enhancing the stability of neurofilament light chain mRNA (Fiesel et al., 2010; Kim et al., 2010; Strong et al., 2007). Our present results indicate that both total and cytoplasmic number of HDAC6 cells were also upregulated after tMCAO, with an increasing but distinct trend from that of TDP-43 (Fig. 4a–c). In other words, HDAC6 and TDP-43 are thought to regulate each other's expression levels, although there is a time lag in their expression levels in the acute ischemic mice model.

The ubiquitin-proteasome system (UPS), a proteolytic pathway that is part of the cellular quality control network, maintains the integrity of the cellular proteome (Ciechanover et al., 2015; Lei et al., 2021). RAD23B acts as a substrate-shuttling factor for the proteasome. Multivalent interactions between RAD23B and ubiquitin chains trigger an LLPS, which then modulates proteasome function (Lei et al., 2021; Sun et al., 2018; Yasuda et al., 2020). Previous studies have shown that ubiquitination of misfolded or mislocalized TDP-43 occurs, not only in ALS and FTLD, but also in stroke disease models (Arai et al., 2006; Kanazawa et al., 2011; Mackenzie et al., 2010; Neumann et al., 2006; Thammisetty et al., 2018). In this study, we observed an increase in the expression of RAD23B and its colocalization with TDP-43 in ischemic mice brains, indicating that RAD23B may promote the proteolytic pathways of mislocalized TDP-43 in a proteasomal-dependent manner in the acute stroke mouse brain (Fig. 5a–e).

G3BP1 is a core nucleating factor for SGs, and HDAC6 acts as a component of SGs. Stress from ischemia mislocalizes TDP-43 in the nucleus and is considered toxic for neurons (Li et al., 2022; Chhangani et al., 2021; Kahl et al., 2018). Therefore, SGs induced by increased expression levels of G3BP1, HDAC6, or both may be responsible for the clearance of mislocalized TDP-43. The co-localization of TDP-43 and G3BP1 after cerebral infarction (Fig. 3) and the increase in HDAC6 (Fig. 4) may be related to the process of TDP-43 clearance. In contrast, the level of expression of G3BP1 and HDAC6 differ after ischemic stroke. G3BP1 only responds to prolonged ischemia (60 min), whereas HDAC6 is up-regulated in response to mild ischemia (30 min), similar to TDP-43. This may be due to the recognition of ubiquitinated TDP-43 by HDAC6 and the incorporation of the former into SGs, whereas G3BP1 maintains a constant level of expression and constantly forms and degrades stress granules (Aramburu-Núñez et al., 2022; Fazal et al., 2021; Liu et al., 2021; Protter et al., 2016). In other words, TDP-43 mislocalized by ischemia may be incorporated into SGs that form around G3BP1 by binding to HDAC6, and ultimately becoming degraded.

Collectively, we observed the mislocalization of TDP-43 in the tMCAO mouse model, as in previous studies (Kahl et al., 2018; Liu et al., 2020). Moreover, we suggest that mislocalized TDP-43 can interact with G3BP1 and/or HDAC6, that it is subsequently stored in SGs, and finally degraded by the UPS. We demonstrated a possible link between ischemic stroke and neurodegenerative disease from the perspective of TDP-43 proteinopathy.

CRediT authorship contribution statement

An Hangping: Investigation. **Liu Hongzhi:** Investigation. **Hu Xiao:** Investigation. **Zhai Yun:** Investigation. **Yu Haibo:** Investigation. **Sun Hongming:** Investigation. **Bian Zhihong:** Investigation. **Yamashita Toru:** Writing – review & editing, Supervision, Resources, Methodology, Investigation, Funding acquisition, Conceptualization. **Ota-Elliott Ricardo Satoshi:** Methodology, Investigation. **Hu Xinran:** Investigation. **Morihara Ryuta:** Supervision, Resources, Conceptualization. **Bian Yuting:** Writing – original draft, Software, Project administration, Investigation, Formal analysis, Data curation, Conceptualization. **Ishiura Hiroyuki:** Writing – review & editing, Supervision, Resources, Methodology, Conceptualization. **Fukui Yusuke:** Writing – review & editing, Supervision, Resources, Methodology, Investigation, Conceptualization.

Declaration of Competing Interest

The authors declare that they have no known competing financial interests or personal relationships that could have appeared to influence the work reported in this paper.

Acknowledgments

This work was supported by JSPS KAKENHI Grant Numbers JP23K08543, JP24K14748 and Grant for Evidence Creation and Basic Research Promotion by the Japanese Society of Cerebral Blood Flow and Metabolism.

References

Abe, K., Kawagoe, J., Araki, T., Aoki, M., Kogure, K., 1992. Differential expression of heat shock protein 70 gene between the cortex and caudate after transient focal cerebral ischaemia in rats. Neurol. Res. 14 (5), 381–385.

Arai, T., Hasegawa, M., Akiyama, H., Ikeda, K., Nonaka, T., Mori, H., Mann, D., Tsuchiya, K., Yoshida, M., Hashizume, Y., Oda, T., 2006. TDP-43 is a component of ubiquitin-positive tau-negative inclusions in frontotemporal lobar degeneration and amyotrophic lateral sclerosis. Biochem Biophys. Res. Commun. 351 (3), 602–611.

Aramburu-Núñez, M., Custodia, A., Pérez-Mato, M., Iglesias-Rey, R., Campos, F., Castillo, J., Ouro, A., Romaus-Sanjurjo, D., Sobrino, T., 2022. Stress granules and acute ischemic stroke: beyond mRNA translation. Int J. Mol. Sci. 23 (7), 3747.

Arimoto-Matsuzaki, K., Saito, H., Takekawa, M., 2016. TIA1 oxidation inhibits stress granule assembly and sensitizes cells to stress-induced apoptosis. Nat. Commun. 7, 10252.

Barmada, S.J., Finkbeiner, S., 2010. Pathogenic TARDBP mutations in amyotrophic lateral sclerosis and frontotemporal dementia: disease-associated pathways. Rev. Neurosci. 21 (4), 251–272.

Boeynaems, S., Alberti, S., Fawzi, N.L., Mittag, T., Polymenidou, M., Rousseau, F., Schymkowitz, J., Shorter, J., Wolozin, B., Van Den Bosch, L., Tompa, P., Fuxreiter, M., 2018. Protein phase separation: a new phase in cell biology. Trends Cell Biol. 28 (6), 420–435.

Chhangani, D., Martín-Peña, A., Rincon-Limas, D.E., 2021. Molecular, functional, and pathological aspects of TDP-43 fragmentation. iScience 24 (5), 102459.

Ciechanover, A., Kwon, Y.T., 2015. Degradation of misfolded proteins in neurodegenerative diseases: therapeutic targets and strategies. Exp. Mol. Med. 47 (3), e147.

Ederle, H., Dormann, D., 2017. TDP-43 and FUS en route from the nucleus to the cytoplasm. FEBS Lett. 591 (11), 1489–1507.

Fazal, R., Boeynaems, S., Swijsen, A., De Decker, M., Fumagalli, L., Moisse, M., Vanneste, J., Guo, W., Boon, R., Vercruysse, T., Eggermont, K., Swinnen, B., Beckers, J., Pakravan, D., Vandoorne, T., Vanden Berghe, P., Verfaillie, C., Van Den Bosch, L., Van Damme, P., 2021. HDAC6 inhibition restores TDP-43 pathology and axonal transport defects in human motor neurons with TARDBP mutations. EMBO J. 40 (7), e106177.

Fiesel, F.C., Voigt, A., Weber, S.S., Van den Haute, C., Waldenmaier, A., Görner, K., Walter, M., Anderson, M.L., Kern, J.V., Rasse, T.M., Schmidt, T., Springer, W., Kirchner, R., Bonin, M., Neumann, M., Baekelandt, V., Alunni-Fabbroni, M., Schulz, J.B., Kahle, P.J., 2010. Knockdown of transactive response DNA-binding protein (TDP-43) downregulates histone deacetylase 6. EMBO J. 29 (1), 209–221.

Guillén-Boixet, J., Kopach, A., Holehouse, A.S., Wittmann, S., Jahnel, M., Schlüßler, R., Kim, K., Trussina, I.R.E.A., Wang, J., Mateju, D., Poser, I., Maharana, S., Ruer-Gruß, M., Richter, D., Zhang, X., Chang, Y.T., Guck, J., Honigmann, A., Mahamid, J., Hyman, A.A., Franzmann, T.M., 2020. RNA-induced conformational switching and clustering of G3BP drive stress granule assembly by condensation. Cell 181 (2), 346–361.e17.

Kahl, A., Blanco, I., Jackman, K., Baskar, J., Milaganur Mohan, H., Rodney-Sandy, R., Zhang, S., Iadecola, C., Hochrainer, K., 2018. Cerebral ischemia induces the aggregation of proteins linked to neurodegenerative diseases. Sci. Rep. 8 (1), 2701.

Kanazawa, M., Kakita, A., Igarashi, H., Takahashi, T., Kawamura, K., Takahashi, H., Nakada, T., Nishizawa, M., Shimohata, T., 2011. Biochemical and histopathological alterations in TAR DNA-binding protein-43 after acute ischemic stroke in rats. J. Neurochem 116 (6), 957–965.

Kawaguchi, Y., Kovacs, J.J., McLaurin, A., Vance, J.M., Ito, A., Yao, T.P., 2003. The deacetylase HDAC6 regulates aggresome formation and cell viability in response to misfolded protein stress. Cell 115 (6), 727–738.

Keating, S.S., San Gil, R., Swanson, M.E.V., Scotter, E.L., Walker, A.K., 2022. TDP-43 pathology: from noxious assembly to therapeutic removal. Prog. Neurobiol. 211, 102229.

Kim, H.J., Raphael, A.R., LaDow, E.S., McGurk, L., Weber, R.A., Trojanowski, J.Q., Lee, V.M., Finkbeiner, S., Gitler, A.D., Bonini, N.M., 2014. Therapeutic modulation of eIF2α phosphorylation rescues TDP-43 toxicity in amyotrophic lateral sclerosis disease models. Nat. Genet. 46 (2), 152–160.

Kim, S.H., Shanware, N.P., Bowler, M.J., Tibbetts, R.S., 2010. Amyotrophic lateral sclerosis-associated proteins TDP-43 and FUS/TLS function in a common biochemical complex to co-regulate HDAC6 mRNA. J. Biol. Chem. 285 (44), 34097–34105.

Kwon, S., Zhang, Y., Matthias, P., 2007. The deacetylase HDAC6 is a novel critical component of stress granules involved in the stress response. Genes Dev. 21 (24), 3381–3394.

Lee, S., Kwon, Y., Kim, S., Jo, M., Jeon, Y.M., Cheon, M., Lee, S., Kim, S.R., Kim, K., Kim, H.J., 2020. The role of HDAC6 in TDP-43-induced neurotoxicity and UPS impairment. Front Cell Dev. Biol. 8, 581942.

Lei, L., Wu, Z., Winklhofer, K.F., 2021. Protein quality control by the proteasome and autophagy: a regulatory role of ubiquitin and liquid-liquid phase separation. Matrix Biol. 100-101, 9–22.

Li, X., Li, R., Lu, L., Dhar, A., Sheng, H., Yang, W., 2022. Beneficial effects of neuronal ATF6 activation in permanent ischemic stroke. Front Cell Neurosci. 16, 1016391.

Liu, P., Xiao, J., Wang, Y., Song, X., Huang, L., Ren, Z., Kitazato, K., Wang, Y., 2021. Posttranslational modification and beyond: interplay between histone deacetylase 6 and heat-shock protein 90. Mol. Med. (Camb., Mass.) 27 (1), 110.

Liu, X., Yamashita, T., Shi, X., Bian, Y., Bian, Z., Omote, Y., Takemoto, M., Hishikawa, N., Ohta, Y., Abe, K., 2020. Dynamic changes and mislocalizations of neurodegenerative disease-related proteins in mice stroke model. Brain Res. 1742, 146862.

Mackenzie, I.R., Neumann, M., Bigio, E.H., Cairns, N.J., Alafuzoff, I., Kril, J., Kovacs, G. G., Ghetti, B., Halliday, G., Holm, I.E., Ince, P.G., Kamphorst, W., Revesz, T., Rozemuller, A.J., Kumar-Singh, S., Akiyama, H., Baborie, A., Spina, S., Dickson, D. W., Trojanowski, J.Q., Mann, D.M., 2010. Nomenclature and nosology for neuropathologic subtypes of frontotemporal lobar degeneration: an update. Acta Neuropathol. 119 (1), 1–4.

McDonald, K.K., Aulas, A., Destroismaisons, L., Pickles, S., Beleac, E., Camu, W., Rouleau, G.A., Vande Velde, C., 2011. TAR DNA-binding protein 43 (TDP-43) regulates stress granule dynamics via differential regulation of G3BP and TIA-1. Hum. Mol. Genet. 20 (7), 1400–1410.

Nakano, Y., Yamashita, T., Li, Q., Sato, K., Ohta, Y., Morihara, R., Hishikawa, N., Abe, K., 2017. Time-dependent change of in vivo optical imaging of oxidative stress in a mouse stroke model. J. Neurosci. Res. 95 (10), 2030–2039.

Neumann, M., Sampathu, D.M., Kwong, L.K., Truax, A.C., Micsenyi, M.C., Chou, T.T., Bruce, J., Schuck, T., Grossman, M., Clark, C.M., McCluskey, L.F., Miller, B.L., Masliah, E., Mackenzie, I.R., Feldman, H., Feiden, W., Kretzschmar, H.A., Trojanowski, J.Q., Lee, V.M., 2006. Ubiquitinated TDP-43 in frontotemporal lobar degeneration and amyotrophic lateral sclerosis. Science 314 (5796), 130–133.

Popp, A., Jaenisch, N., Witte, O.W., Frahm, C., 2009. Identification of ischemic regions in a rat model of stroke. PLoS One 4 (3), e4764.

Prasad, A., Bharathi, V., Sivalingam, V., Girdhar, A., Patel, B.K., 2019. Molecular mechanisms of TDP-43 misfolding and pathology in amyotrophic lateral sclerosis. Front Mol. Neurosci. 12, 25.

Protter, D.S.W., Parker, R., 2016. Principles and properties of stress granules. Trends Cell Biol. 26 (9), 668–679.

Sanders, D.W., Kedersha, N., Lee, D.S.W., Strom, A.R., Drake, V., Riback, J.A., Bracha, D., Eeftens, J.M., Iwanicki, A., Wang, A., Wei, M.T., Whitney, G., Lyons, S.M., Anderson, P., Jacobs, W.M., Ivanov, P., Brangwynne, C.P., 2020. Competing protein-RNA interaction networks control multiphase intracellular organization. Cell 181 (2), 306–324. .e28.

Schärer, O.D., 2013. Nucleotide excision repair in eukaryotes. Cold Spring Harb. Perspect. Biol. 5 (10), a012609.

Scotter, E.L., Chen, H.J., Shaw, C.E., 2015. TDP-43 Proteinopathy and ALS: Insights into disease mechanisms and therapeutic targets. Neurotherapeutics 12 (2), 352–363.

Shang, J., Yan, H., Jiao, Y., Ohta, Y., Liu, X., Li, X., Morihara, R., Nakano, Y., Fukui, Y., Shi, X., Huang, Y., Feng, T., Takemoto, M., Sato, K., Hishikawa, N., Yamashita, T., Abe, K., 2018. Therapeutic effects of pretreatment with tocovid on oxidative stress in postischemic mice brain. J. Stroke Cereb. Dis. 27 (8), 2096–2105.

Shenouda, M., Zhang, A.B., Weichert, A., Robertson, J., 2018. Mechanisms associated with TDP-43 neurotoxicity in ALS/FTLD. Adv. Neurobiol. 20, 239–263.

Shibahara, T., Ago, T., Nakamura, K., Tachibana, M., Yoshikawa, Y., Komori, M., Yamanaka, K., Wakisaka, Y., Kitazono, T., 2020. Pericyte-mediated tissue repair through PDGFRβ promotes peri-infarct astrogliosis, oligodendrogenesis, and functional recovery after acute ischemic stroke. eNeuro 7 (2), ENEURO.0474-19.2020.

Si, W., Li, Z., Huang, Z., Ye, S., Li, X., Li, Y., Kuang, W., Chen, D., Zhu, M., 2020. RNA binding protein motif 3 inhibits oxygen-glucose deprivation/reoxygenation-induced apoptosis through promoting stress granules formation in PC12 cells and rat primary cortical neurons. Front Cell Neurosci. 14, 559384.

Sidibé, H., Dubinski, A., Vande Velde, C., 2021. The multi-functional RNA-binding protein G3BP1 and its potential implication in neurodegenerative disease. J. Neurochem. 157 (4), 944–962.

Strong, M.J., Volkening, K., Hammond, R., Yang, W., Strong, W., Leystra-Lantz, C., Shoesmith, C., 2007. TDP43 is a human low molecular weight neurofilament (hNFL) mRNA-binding protein. Mol. Cell Neurosci. 35 (2), 320–327.

Suk, T.R., Rousseaux, M.W.C., 2020. The role of TDP-43 mislocalization in amyotrophic lateral sclerosis. Mol. Neurodegener. 15 (1), 45.

Sun, D., Wu, R., Zheng, J., Li, P., Yu, L., 2018. Polyubiquitin chain-induced p62 phase separation drives autophagic cargo segregation. Cell Res 28 (4), 405–415.

Tachibana, M., Ago, T., Wakisaka, Y., Kuroda, J., Shijo, M., Yoshikawa, Y., Komori, M., Nishimura, A., Makihara, N., Nakamura, K., Kitazono, T., 2017. Early reperfusion after brain ischemia has beneficial effects beyond rescuing neurons. Stroke 48 (8), 2222–2230.

Thammisetty, S.S., Pedragosa, J., Weng, Y.C., Calon, F., Planas, A., Kriz, J., 2018. Age-related deregulation of TDP-43 after stroke enhances NF-κB-mediated inflammation and neuronal damage. J. Neuroinflamm. 15 (1), 312.

Watanabe, S., Inami, H., Oiwa, K., Murata, Y., Sakai, S., Komine, O., Sobue, A., Iguchi, Y., Katsuno, M., Yamanaka, K., 2020. Aggresome formation and liquid-liquid phase separation independently induce cytoplasmic aggregation of TAR DNA-binding protein 43. Cell Death Dis. 11 (10), 909.

Wolozin, B., Ivanov, P., 2019. Stress granules and neurodegeneration. Nat. Rev. Neurosci. 20 (11), 649–666.

Yamashita, T., Ninomiya, M., Hernández Acosta, P., García-Verdugo, J.M., Sunabori, T., Sakaguchi, M., Adachi, K., Kojima, T., Hirota, Y., Kawase, T., Araki, N., Abe, K., Okano, H., Sawamoto, K., 2006. Subventricular zone-derived neuroblasts migrate and differentiate into mature neurons in the post-stroke adult striatum. J. Neurosci. 26 (24), 6627–6636.

Yang, P., Mathieu, C., Kolaitis, R.M., Zhang, P., Messing, J., Yurtsever, U., Yang, Z., Wu, J., Li, Y., Pan, Q., Yu, J., Martin, E.W., Mittag, T., Kim, H.J., Taylor, J.P., 2020. G3BP1 is a tunable switch that triggers phase separation to assemble stress granules. Cell 181 (2), 325–345. .e28.

Yasuda, S., Tsuchiya, H., Kaiho, A., Guo, Q., Ikeuchi, K., Endo, A., Arai, N., Ohtake, F., Murata, S., Inada, T., Baumeister, W., Fernández-Busnadiego, R., Tanaka, K., Saeki, Y., 2020. Stress- and ubiquitylation-dependent phase separation of the proteasome. Nature 578 (7794), 296–300.